排灌机械工程学报 2018 年 4 月 Apr. 2018 第 36 卷 第 4 期 Vol. 36 No. 4
Journal of Drainage and Irrigation Machinery Engineering

Doi: 10.3969/j. issn.1674 - 8530.16.1049

Numerical simulation of cavitation around a Clark - Y hydrofoil with different LES models in OpenFOAM

ZHU Ziming

ZHU Ziming*, QIAN Zhongdong, GUO Zhiwei, YANG Bing
(State Key Laboratory of Water Resources and Hydropower Engineering Science, Wuhan University, Wuhan, Hubei 430072, China)

Abstract: A finite volume, multiphase solver in the framework of OpenFOAM was used to calculate the flow field of the cavitating flow over the Clark - Y hydrofoil. This solver used Transport Based Equation Model (TEM) to solve the liquid volume fraction, and utilized volume of fluid (VOF) technique to predict the interface between liquid and vapor phases. The simulation was designed to study the cavitation shedding and different fluid characteristics in the cloud cavitation regime when adopting two different Large Eddy Simulation (LES) models, namely, one equation eddy viscosity (oneEqEddy) model and Smagorinsky model. It is shown that these two models can be used to study the cavitation shedding dynamics and predict the velocity profiles.

Key words: hydrofoil; cavitation; OpenFOAM; Large Eddy Simulation
CLC Number: S277.9 **Document Code**: A **Article No**: 1674 - 8530(2018)04 - 0277 - 06

ZHU Ziming, QIAN Zhongdong, GUO Zhiwei, et al. Numerical simulation of cavitation around a Clark - Y hydrofoil with different LES models in OpenFOAM(JDIME), 2018,36(4):277 - 282.

1 Introduction

Cavitation is usually defined as the breakdown of a liquid medium under the saturated vapor pressure[1]. This dynamic process can be found in marine propellers, pumps, hydrofoils and other hydraulic machineries by observing the formation, growth and collapse of vapor bubbles. A comprehensive understanding of the cavitation shedding is of crucial importance to explaining the vibration, erosion and power loss of hydraulic machinery operating under cavitating conditions.

The sharp changes in the fluid density, and the requirement of modelling phase change were the factors in numerical simulation of cavitation flows[2]. According to the assumption of a homogenous equilibrium medium proposed by JI et al[3], the vapor and liquid phases were considered as homogeneous mixture in order to solve only one set of equations for the mass and momentum. SAUER[4] proposed the equations by making some improvements of the Rayleigh equation, while MERKLE et al[5] and KUNZ et al[6] presented semi-analytical equations.

The interface between liquid and vapor was tracked by the volume of fluid (VOF) method, in which the volume fraction function γ was defined[7]. Many researchers have used this method to capture the cavity shape for its accuracy and robustness. For example, PENG et al[8] and BENSOW et al[9] used the VOF technology to simulate cavitation over hydrofoils and propellers respectively.

The simulation was associated with the experi-

Received date: 2016 - 12 - 09; **Accepted date**: 2017 - 03 - 14; **Publish time on line**: 2018 - 03 - 02
Online Publishing: http://kns.cnki.net/kcms/detail/32.1814.TH.20180302.1107.198.html
First author: ZHU Ziming (1992—), male, master(corresponding author, zimingzhu1992@163.com), researching in turbomachinery, numerical simulation.
Second author: QIAN Zhongdong (1976—), male, professor(zdqian@whu.edu.com), researching in turbomachinery, numerical simulation.

ments conducted by WANG et al[10], in which hairpin type of counter-rotating vapor vortices were observed at incipient cavitation, and large-scale vortex structure and rear re-entrant jet were found at cloud cavitation. HUANG et al[11], simulated the cavitating flow over the Clark – Y hydrofoil with Partially Averaged Navier – Stocks (PANS) model and proved the consistency between the simulation and experiments. Meanwhile, JOHAN et al[12] discussed the cavitation dynamics by different cavitating numbers and cavitation models with the same Large Eddy Simulation (LES) turbulence model. LES was based on resolving the large-scale eddies while modelling subgrid-scales. Many reviews indicated that both accurate discretization methods and the subgrid-scale models were important factors in LES[12].

In the present study, a finite volume, multiphase solver in the framework of OpenFOAM is also used to calculate the flow field of the cavitating flow over a Clark – Y hydrofoil by adopting two different subgrid-scale (SGS) models, namely, one equation eddy viscosity (oneEqEddy) and Smagorinsky in order to find a suitable model.

2 Numerical models

2.1 VOF Model

In the paper, γ is the fraction of water volume, $\gamma=0$ denotes vapor and $\gamma=1$ is liquid. Cells which lie between 0 and 1 contain interface regions. This can be written as[13]

$$\gamma(x,t)=\begin{cases}0, & \text{Vapor phase}\\ 0<\gamma<1, & \text{Liquid – vapor region}\\ 1. & \text{Liquid phase}\end{cases} \quad (1)$$

An improved version of "The Compressive Interface Capturing Scheme for Arbitrary Meshes (CICSAM)" VOF technique[2] is used in OpenFOAM, which is defined as

$$\frac{\partial\gamma}{\partial t}+\nabla\cdot(\gamma\boldsymbol{v})+\nabla\cdot[\boldsymbol{v}_c\gamma(1-\gamma)]=0, \quad (2)$$

$$\boldsymbol{v}_c=\min[C_\gamma|\boldsymbol{v}|,\max|\boldsymbol{v}|]\frac{\nabla\gamma}{|\nabla\gamma|}, \quad (3)$$

where $\boldsymbol{v}_c$ is interface-compressive velocity, and C_γ is a constant defining the intensity of the compression.

2.2 Transport based equation model

The mixture density ρ and the turbulent viscosity μ are defined, respectively, as follows

$$\rho=\gamma\rho_l+(1-\gamma)\rho_v, \quad (4)$$

$$\mu=\gamma\mu_l+(1-\gamma)\mu_v. \quad (5)$$

The transport equation for the phase change is

$$\frac{\partial\gamma}{\partial t}+\nabla\cdot(\gamma\boldsymbol{v})=\frac{\dot{m}}{\rho_l}. \quad (6)$$

The specific interphase mass transfer rate $\dot{m}$ in Schnerr – Sauer Model is given as below

$$\begin{cases}\dot{m}^+=C_e\dfrac{3\rho_v\rho_l}{\rho R}\gamma(1-\gamma)\sqrt{\dfrac{2(p_v-p)}{3\rho_l}},\\ \dot{m}^-=C_c\dfrac{3\rho_v\rho_l}{\rho R}\gamma(1-\gamma)\sqrt{\dfrac{2(p-p_v)}{3\rho_l}}.\end{cases} \quad (7)$$

where R is the radius of the bubbles, p_v is the saturated vapor pressure, C_e and C_c are coefficients related to processes of condensation and vaporization[14].

2.3 Large Eddy Simulation

The cutoff filter can be written as

$$\bar{\phi}=\int_D\phi G(x,x')\,\mathrm{d}x. \quad (8)$$

Applying the filter (8) to the Navier – Stokes equations, the filtered equations are expressed as

$$\frac{\partial p}{\partial t}+\nabla\cdot(\rho\bar{\boldsymbol{v}})=0, \quad (9)$$

$$\frac{\partial(\rho\bar{\boldsymbol{v}})}{\partial t}+\nabla\cdot(\rho\bar{\boldsymbol{v}}\times\bar{\boldsymbol{v}})=-\nabla\bar{p}+\nabla\cdot(\bar{s}-B), \quad (10)$$

where $D=\frac{1}{2}(\nabla\boldsymbol{v}+\nabla\boldsymbol{v}^{\mathrm{T}})$ is the rate-of-strain tensor, $\bar{s}=2\mu\bar{D}$ is the viscous stress tensor, $B=(\overline{\boldsymbol{v}\times\boldsymbol{v}}-\bar{\boldsymbol{v}}\times\bar{\boldsymbol{v}})$ is the subgrid stress tensor and can be computed in a wide variety of SGS models.

In Smagorinsky model and oneEqEddy model, the filters are carried out implicitly with the filter width Δ defined by the grid based on the assumption that the deviatoric part of the subgrid stress tensor, $B_D=B-\frac{2}{3}kI$ and the deviatoric part of the rate-of-strain tensor are aligned, such as that, $B_D\approx-2v_k\bar{D}$[15].

In Smagorinsky model v_{sgs} is defined as

$$v_{sgs}=C_D\Delta^2|\tilde{S}|. \quad (11)$$

In oneEqEddy model v_{sgs} is modeled as $v_{sgs}=C_k\Delta\sqrt{k}$, with k being the solution of

$$\frac{\partial k}{\partial t} + \nabla \cdot (k\bar{v}) = -B \cdot \tilde{S} + \nabla \cdot (v_{sgs} \nabla k) - C_\varepsilon \frac{k^{\frac{3}{2}}}{\Delta}, \tag{12}$$

where C_D, C_k and C_ε are model coefficients.

3 Mesh generation and calculation conditions

As illustrated in Fig. 1, the computation domain represents the test section part of the cavitation tunnel. The two-dimensional Clark – Y hydrofoil was clamped on both sides of the tunnel walls and certain cavitation number can be reached by a regulation system. The chord length of the hydrofoil is $c = 0.07$ m and the attack angle equals 8°.

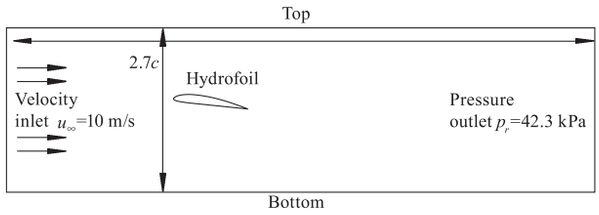

Fig. 1 Geometry of computation domain

Structured grid was used in the whole domain and the C-type meshes were generated near the wall of the hydrofoil. The grid was created in ICEM software with 246 813 cells and then converted into the format for that OpenFOAM. The meshes around the hydrofoil were refined to ensure that the maximum value of y^+ was less than one as shown in Fig. 2.

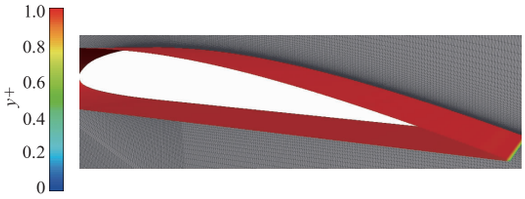

Fig. 2 Refined meshes and y^+ around the hydrofoil

Two non-dimensional numbers, Reynolds number (Re) and cavitation number σ, define the calculation condition.

$$Re = \frac{u_\infty c}{v}, \tag{13}$$

$$\sigma = \frac{p_r - p_v}{\frac{\rho u_\infty^2}{2}}, \tag{14}$$

where u_∞ is the free stream velocity, v is the kinematic viscosity of water at constant temperature of 293 K, ρ is the density of water, and the saturated vapor pressure of water p_v equals 2.34 kPa.

When decreasing the cavitation number, four different types of cavitation can be classified by the cavity length and shape, in which cloud cavitation accompanied by the highly unsteady trailing edge and vortex shedding has been a hot topic in hydrodynamic field. According to the experiments conducted by WANG et al[10], cloud cavitation was formed when the Reynolds number equals 7.0×10^5 and the cavitation number σ was 0.8, therefore, we can have the calculation conditions as described in Tab. 1.

Tab. 1 Boundary conditions of the simulation

Patch	Boundary conditions
Inlet	Velocity inlet u_∞ = 10 m/s
Outlet	Pressure outlet p_r = 42.3 kPa
Top and bottom	No slip
Front and back	Empty
Hydrofoil	No slip

The cavitation mass transfer model in numerical simulations was Schnerr – Sauer. The only difference between simulations was the application of oneEqEddy subgrid-scale model and Smagorinsky subgrid-scale model. The pressure implicit with splitting of operators (PISO) algorithm was used to solve the governing equations and the maximum courant number was set to be 0.6 by adopting adaptive time step.

4 Results and discussion

The lift coefficient C_L and the drag coefficient C_D are defined as

$$C_L = \frac{L}{\frac{\rho u_\infty^2}{2}}, \tag{15}$$

$$C_D = \frac{D}{\frac{\rho u_\infty^2}{2}}, \tag{16}$$

where u_∞ is the free stream velocity, ρ is the density of water, L is the lift force exerted upon the hydrofoil and D is the drag force.

Since lift force is generated by the pressure difference between the cavity and the hydrodynamic pres-

sure, the lift coefficient will increase in pace with the cavity length. However, after cavity length reaches its maximum, the pressure distribution at the trailing edge of the hydrofoil is influenced by the cavity shedding, which results in the oscillation of the lift coefficients. Fig. 3 shows the variation of lift coefficients on one cavitation cycle using two models in addition to experimental data in reference [10].

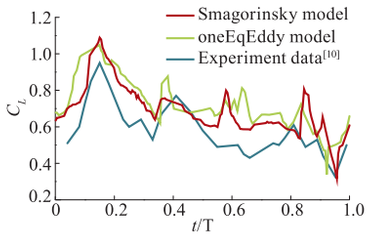

Fig. 3 Variation of lift coefficient with time

As shown in Fig. 3, two SGS models over predict the maximum lift coefficients although the minimum lift coefficients are nearly equal. Besides, oneEqEddy model predicts more complex oscillatory peaks and the result of Smagorinsky model has a better consistence with that of experiments. The averages of lift and drag coefficients on one cavitation cycle between experiments and the simulation are presented in Tab. 2. Results of the two SGS models indicate that different SGS models predict different averages of force coefficients and the drag coefficient of the simulation is inaccurate because the maximum error is about 20%. Remarkably, the maximum error of oneEqEddy model in reference [2] is 16.66%, this disparity may be caused by the different parameters used in the simulation and measured in the experiment such as average diameter of nuclei and number of nuclei per volume.

Tab. 2 Averages of lift and drag coefficients

	C_L	*Error*/%
Smagorinsky	0.690	9.2
oneEqEddy	0.720	5.3
Experiment[10]	0.760	–
	C_D	*Error*/%
Smagorinsky	0.143	19.2
oneEqEddy	0.141	17.5
Experiment[10]	0.120	–

Time-averaged velocity distribution at different locations is one of the important factors to study the flow details. The LDV measurements start from the surface point of the hydrofoil which are located at $x/c = 20\%$, 40%, 60%, 80%, 100%, 120% and end near $y = 0.025$ m. When we consider the difficulties in measuring the velocity profiles near the closure region, it is more representative to compare the CFD results with experiment data in the middle part of the hydrofoil. Detailed information of velocity profiles at $x/c = 40\%$ and $x/c = 60\%$ is illustrated in Fig. 4 and Fig. 5 respectively. From the numerical results, the ordinate of the maximum velocity is about $y = 0.01$ m, Smagorinsky model predicts higher velocity than oneEqEddy model when the value is higher than 0.01. According to the velocity profiles in Fig. 5, there is reverse flow and the velocity of OneEqEddy model is slightly higher than that of Smagorinsky model in the near-wall region.

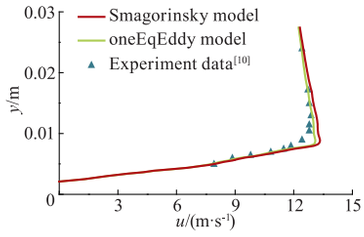

Fig. 4 Time-averaged velocity at $x/c = 40\%$

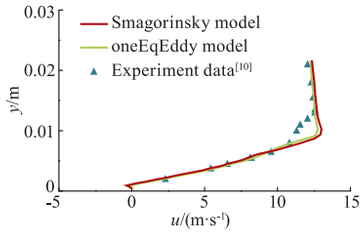

Fig. 5 Time-averaged velocity at $x/c = 60\%$

Comparing the two SGS models with the experiment data, it is clear that there is a great difference near the inflection point of the curve. This region is the interface between liquid and vapor phases based on the estimated thickness in reference [10]. This disparity between the simulation and experiment is greater along the direction of flow in the middle part of the hydrofoil. In the near-wall region, the velocity profiles calculated by these two SGS models are consistent with experiment data and the difference between out-of-cavity flow velocities with these two models is minimal.

According to the experimental results of reference [10], time evolution of cloud cavitation from the side

view is shown in Fig. 6. The frames in Fig. 6 show the cavitation cycle as follows[2]

1) Cavity appears at the leading edge of the hydrofoil.

2) Cavity grows until it occupies most of the hydrofoil.

3) The massive cavity shedding appears and a re-entrant jet can be observed.

4) Cavity begins to disappear.

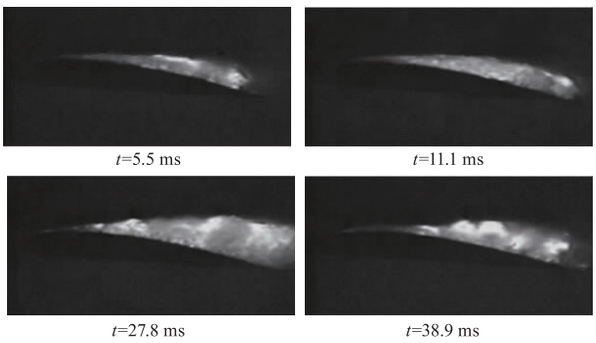

Fig. 6 Time evolution of the cloud cavitation from the side view[10]

Fig. 7 presents cavitation dynamics of oneEqEddy (left) model and Smagorinsky (right) model.

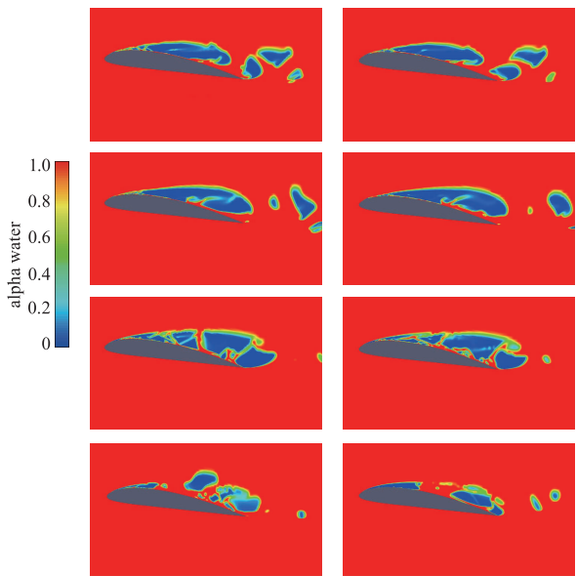

Fig. 7 Contour of the fraction of liquid γ, oneEqEddy (left) and Smagorinsky (right)

Based on the results, the following features can be concluded:

1) Different SGS models predict different cavity structures and the difference between oneEqEddy model and Smagorinsky model is greater over time.

2) The re-entrant jet can be observed in both SGS models.

3) The cavity structure at the trailing edge of OneEqEddy model is more complicated.

Pressure contours of oneEqEddy (left) model and Smagorinsky (right) model are illustrated in Fig. 8. Based on the comparison and analysis, some findings are listed as below:

1) Low-pressure area mainly distributes along the hydrofoil, there is little difference before cavity shedding between oneEqEddy model and Smagorinsky model.

2) A local-high pressure region exists near the trailing edge of the hydrofoil.

3) The Smagorinsky model predicts higher pressure than oneEqEddy model.

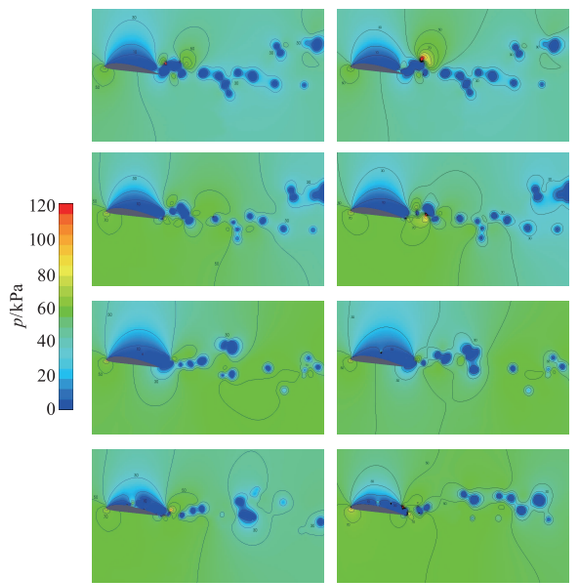

Fig. 8 Contours of pressure, oneEqEddy (left) and Smagorinsky (right)

5 Conclusions

Two subgrid-scale models of LES including the Smagorinsky model and the oneEqEddy model were implemented for predicting the cavitation flow over the Clark – Y hydrofoil. According to the results of the simulation, lift force performs an oscillatory behavior with time and oneEqEddy model predicts a little more accurate lift coefficients than Smagorinsky model, and these two models can be used to predict the velocity

profiles in the cloud cavitation regime.

Acknowledgements

The research was supported by the National Natural Science Foundation of China(No. 51422906).

References

[1] FRANC J P, MICHEL J M. Fundamentals of cavitation [M]. Netherlands:Springer, 2005.

[2] ROOHI E, ZAHIRI A P, PASSANDIDEH-FARD M. Numerical simulation of cavitation around a two-dimensional hydrofoil using VOF method and LES turbulence model[J]. Applied mathematical modelling, 2013, 37(9):6469-6488.

[3] JI B, LUO X W, ARNDT R E A, et al. Large eddy simulation and theoretical investigations of the transient cavitating vortical flow structure around a NACA66 hydrofoil[J]. International journal of multiphase flow, 2015, 68(68):121-134.

[4] SAUER J. Instationaren kaviterendeStromung — Ein neues Modell, baserend auf Front Capturing (VOF) and Blasendynamik[D]. Karlsruhe: Karlsruhe Universitat, 2000.

[5] MERKLE C L, FENG J, BUELOW P E O. Computational modeling of the dynamics of sheet cavitation [C]//Third International Symposium on Cavitation, Grenoble, France, 1998.

[6] KUNZ R F, BOGER D A, STINEBRING D R, et al. A preconditioned Navier-Stokes method for two-phase flows with application to cavitation prediction[J]. Computers & fluids, 2000, 29(8):849-875.

[7] HIRT C W, NICHOLS B D. Volume of fluid (VOF) method for the dynamics of free boundaries[J]. Journal of computational physics, 1981, 39(1):201-225.

[8] PENG X X, JI B, CAO Y, et al. Combined experimental observation and numerical simulation of the cloud cavitation with U-type flow structures on hydrofoils[J]. International journal of multiphase flow, 2016, 79:10-22.

[9] BENSOW R E, BARK G. Simulating cavitating flows with LES in openFOAM[C]//Proceedings of Computational Fluid Dynamics, Lisbon, Portugal, 2010: 14-17.

[10] WANG G, SENOCAK I, WEI S, et al. Dynamics of attached turbulent cavitating flows[J]. Progress in aerospace sciences, 2001, 37(6):551-581.

[11] HUANG B, WANG G Y. Partially averaged Navier-Stokes method for time-dependent turbulent cavitating flows[J]. J. Hydrodyn, 2011, 23(1):26-33.

[12] JOHAN Meyers, MARTINE Baelmans. Determination of subfilter energy in large-eddy simulations[J]. Journal of turbulence, 2004, 527(5):1468-5248.

[13] ASNAGHI A. Interphase change foam tutorial and PANS turbulence model[D]. Chalmers: Chalmers University of Technology, 2013.

[14] BIN J I, LUO X W, PENG X X, et al. Numerical investigation of the ventilated cavitating flow around an under-water vehicle based on a three-component cavitation model[J]. J. Hydrodyn. Ser. B, 2010, 22(6):753-759.

[15] FUREBY C. On the justification and extension of mixed models in LES[J]. Journal of turbulence, 2007, 8(8): 1-17.

(特约编辑 赵凤朝 责任编辑 盛杰)